Molecular Requirements for Duplex Recognition and Cleavage by Eukaryotic RNase III: Discovery of an RNA-dependent DNA Cleavage Activity of Yeast Rnt1p

ARTICLE *in* JOURNAL OF MOLECULAR BIOLOGY · MAY 2004

Impact Factor: 4.33 · DOI: 10.1016/j.jmb.2004.02.059 · Source: PubMed

4 AUTHORS, INCLUDING:

Bruno Lamontagne
Hôpital Maisonneuve-Rosemont
13 PUBLICATIONS **349** CITATIONS
SEE PROFILE

Sherif Abou Elela
Université de Sherbrooke
78 PUBLICATIONS **2,308** CITATIONS
SEE PROFILE

doi:10.1016/j.jmb.2004.02.059 J. Mol. Biol. (2004) 338, 401–418

JMB

Available online at www.sciencedirect.com

SCIENCE DIRECT®

ELSEVIER

Molecular Requirements for Duplex Recognition and Cleavage by Eukaryotic RNase III: Discovery of an RNA-dependent DNA Cleavage Activity of Yeast Rnt1p

Bruno Lamontagne[1], Rami N. Hannoush[2], Masad J. Damha[2] and Sherif Abou Elela[1]*

[1]*Groupe ARN/RNA Group Département de microbiologie et d'infectiologie, faculté de médecine, Université de Sherbrooke, Sherbrooke, Que. Canada J1H 5N4*

[2]*Department of Chemistry McGill University, Montréal Que., Canada, H3A 2K6*

Members of the double-stranded RNA (dsRNA) specific RNase III family are known to use a conserved dsRNA-binding domain (dsRBD) to distinguish RNA *A*-form helices from DNA *B*-form ones, however, the basis of this selectivity and its effect on cleavage specificity remain unknown. Here, we directly examine the molecular requirements for dsRNA recognition and cleavage by the budding yeast RNase III (Rnt1p), and compare it to both bacterial RNase III and fission yeast RNase III (Pac1). We synthesized substrates with either chemically modified nucleotides near the cleavage sites, or with different DNA/RNA combinations, and investigated their binding and cleavage by Rnt1p. Substitution for the ribonucleotide vicinal to the scissile phosphodiester linkage with 2′-deoxy-2′-fluoro-β-D-ribose (2′ F-RNA), a deoxyribonucleotide, or a 2′-*O*-methylribonucleotide permitted cleavage by Rnt1p, while the introduction of a 2′, 5′-phosphodiester linkage permitted binding, but not cleavage. This indicates that the position of the phosphodiester link with respect to the nuclease domain, and not the 2′-OH group, is critical for cleavage by Rnt1p. Surprisingly, Rnt1p bound to a DNA helix capped with an NGNN tetraribonucleotide loop indicating that the binding of at least one member of the RNase III family is not restricted to RNA. The results also suggest that the dsRBD may accommodate *B*-form DNA duplexes. Interestingly, Rnt1p, but not Pac1 nor bacterial RNase III, cleaved the DNA strand of a DNA/RNA hybrid, indicating that *A*-form RNA helix is not essential for cleavage by Rnt1p. In contrast, RNA/DNA hybrids bound to, but were not cleaved by Rnt1p, underscoring the critical role for the nucleotide located at 3′ end of the tetraloop and suggesting an asymmetrical mode of substrate recognition. In cell extracts, the native enzyme effectively cleaved the DNA/RNA hybrid, indicating much broader Rnt1p substrate specificity than previously thought. The discovery of this novel RNA-dependent deoxyribonuclease activity has potential implications in devising new antiviral strategies that target actively transcribed DNA.

*Corresponding author

Keywords: RNase III; DNA cleavage; RNAi; Rnt1p; dsRBD

Introduction

RNA duplexes elicit a variety of cellular responses that vary from gene silencing to triggering a cellular immune response that leads to the inhibition of protein synthesis.[1,2] The presence of double-stranded RNA (dsRNA) may also act as a processing signal that leads to mature stable RNA, such as rRNA or snRNAs.[3,4] Most of the dsRNA functions are mediated by dsRNA-binding

Supplementary data associated with this article can be found at doi: 10.1016/j.jmb.2004.02.059

Present address: R.N. Hannoush, Department of Chemistry and Chemical Biology, Harvard University, 12 Oxford Street, Cambridge, MA 02138, USA.

Abbreviations used: dsRNA, double-stranded RNA; dsRBD, dsRNA-binding domain; IBPB, initial binding and positioning box; BSB, binding stability box; CEB, cleavage efficiency box; TLC, thin-layer chromatography.

E-mail address of the corresponding author: sherif.abou.elela@usherbrooke.ca

proteins (dsRBPs) that share a conserved dsRBD.[5] The structure of the dsRBD reveals a conserved αβββα fold that fits well with the spacing of the *A*-form RNA helix minor groove and not with the *B*-form DNA helix.[6] Despite the high level of specificity observed *in vivo*, most dsRBPs bind RNA duplexes with low sequence specificity *in vitro*,[3,4,7] suggesting that other factors may alter the specificity of dsRBPs *in vivo*.[8] The specific cleavage of dsRNA is carried out by a group of dsRBPs related to the bacterial ribonuclease III (RNase III).[4,9] The functional enzyme is a homodimeric protein that uses Mg^{2+} to introduce two staggered cleavages on each side of the RNA duplex. Binding of the bacterial RNase III usually leads to cleavage, and both events are regulated by antideterminant sequences surrounding the cleavage sites.[10] Bacterial RNase III does not bind to dsDNA nor to DNA/RNA hybrids.[11–13] However, it does cleave chemically synthesized RNA substrates with a 2′-deoxyribose residue located at the scissile phosphodiester bond.[14]

The catalytic mechanism of eukaryotic RNase III is not well understood. It was suggested that bacterial RNase III uses a "two metal ion" mechanism similar to that of alkaline phosphatase, RNase H and certain restriction enzymes.[15,16] Consistent with this thinking RNase III cleaves its substrates with 5′ end polarity,[11,17] and does not require the presence of a 2′-hydroxyl group adjacent to the scissile bond.[14] This is also probably true for the fission yeast orthologue Pac1, which generates products with 5′-phosphoryl and 3′-hydroxyl termini.[18] The crystal structure of bacterial RNase III bound to either Mg^{2+} or Mn^{2+} indicates that the metal ion is bound to three sidechains of negatively charged amino acids and three water molecules.[19] The positions of the water molecules are consistent with a role in catalysis, and appear to be similar to those of the water molecules associated with the metal ions bound to restriction enzymes.[20]

The yeast *Saccharomyces cerevisiae* orthologue of bacterial RNase III, Rnt1p, recognizes RNA capped with a conserved NGNN tetraloop and cleaves at a fixed distance from this loop.[21] Mutations, chemical interference and NMR analysis indicate that Rnt1p binding and cleavage are regulated by reactivity epitopes grouped into three boxes.[22] These are the initial binding and positioning box (IBPB) located at the tetraloop, the binding stability box (BSB) located adjacent to the tetraloop and the cleavage efficiency box (CEB) located near the cleavage site (see Figure 1). Alteration of the sequences of the IBPB and the BSB inhibits cleavage and reduces binding, while alteration of the CEB sequence inhibits cleavage without affecting the binding efficiency. The second nucleotide, of the IBPB is the only universally conserved nucleotide and changing it to any nucleotide other than G reduces binding significantly and blocks cleavage.[23] This indicates that, unlike other dsRBPs, the primary Rnt1p-binding site is an NGNN tetraloop and not an RNA duplex with low sequence complexity.[24] In fact, Rnt1p may use the tetraloop to direct cleavage within both double-stranded and single-stranded RNA fragments,[25] confirming the observation that an *A*-form RNA helix is not required at the cleavage site. However, the effects of the substrate's overall helical shape, and the contribution of the RNA's 2′-OH, to Rnt1p binding and cleavage remain unclear.

Here, we show that Rnt1p requires a 3′–5′ linkage, but not a 2′-OH group, near the scissile bond for cleavage, suggesting that the cleavage is assisted by coordinated water molecules. We also show that an *A*-form RNA helix is not required for either binding or cleavage by Rnt1p, indicating a wider than expected substrate specificity for at least one member of the RNase III family. Substitution of the RNA strand at the 5′-end of the tetraloop with DNA is tolerated, while substitutions either in the tetraloop or the sequence at its 3′-end block cleavage. This indicates that, unlike any other known dsRBPs, Rnt1p binds its substrate in an asymmetrical manner and selectively recognizes one side of the stem-loop structure. Together, the results suggest that Rnt1p recognizes the fold of the tetraloop and its adjacent four nucleotides and not the shape or 2′-OH content of the RNA helix.

Results

Cleavage chemistry, substrate design and synthesis

Cleavage of phosphodiester bonds by both bacterial and fission yeast RNase III generates products with 5′-phosphoryl and 3′-hydroxyl termini at the cleavage site.[11,17,18] Analysis of the 3′ end product generated by Rnt1p using thin-layer chromatography (TLC) indicates that the baker's yeast enzyme also produces a 5′-phosphoryl terminus (Supplementary Figure 1). This suggests that the three different RNase III enzymes use similar cleavage chemistries. In order to further elucidate the nature of the Rnt1p cleavage reaction, and to identify the mechanism that promotes the catalytic hydrolysis of the phosphodiester bond, we chemically synthesized RNA hairpins[26] possessing modified nucleotides at the cleavage sites (Figures 1 and 2). The modified hairpins were initially based on a model substrate ($R_{19}LR_{19}$) adapted from the natural Rnt1p cleavage site found at the 3′ end of U5 snRNA.[27] The modified hairpins include $R_{19(dU)}LR_{19}$ and $R_{19(2'\text{-OMe})}LR_{19}$ in which the uridine residue located on the 5′ side of the cleavage site is replaced by either 2′-deoxyuridine (dU) or 2′-*O*-methyluridine (2′-OMe U), respectively. $R_{19(2'rU)}LR_{19}$ differs from the native $R_{19}LR_{19}$ in that the 3′,5′-phosphodiester bond at the cleavage site is replaced with the isomeric 2′, 5′-phosphodiester bond (Figure 1). In addition, other chimeric deoxyribo/ribo hairpins were synthesized in order to assess the effect of helical

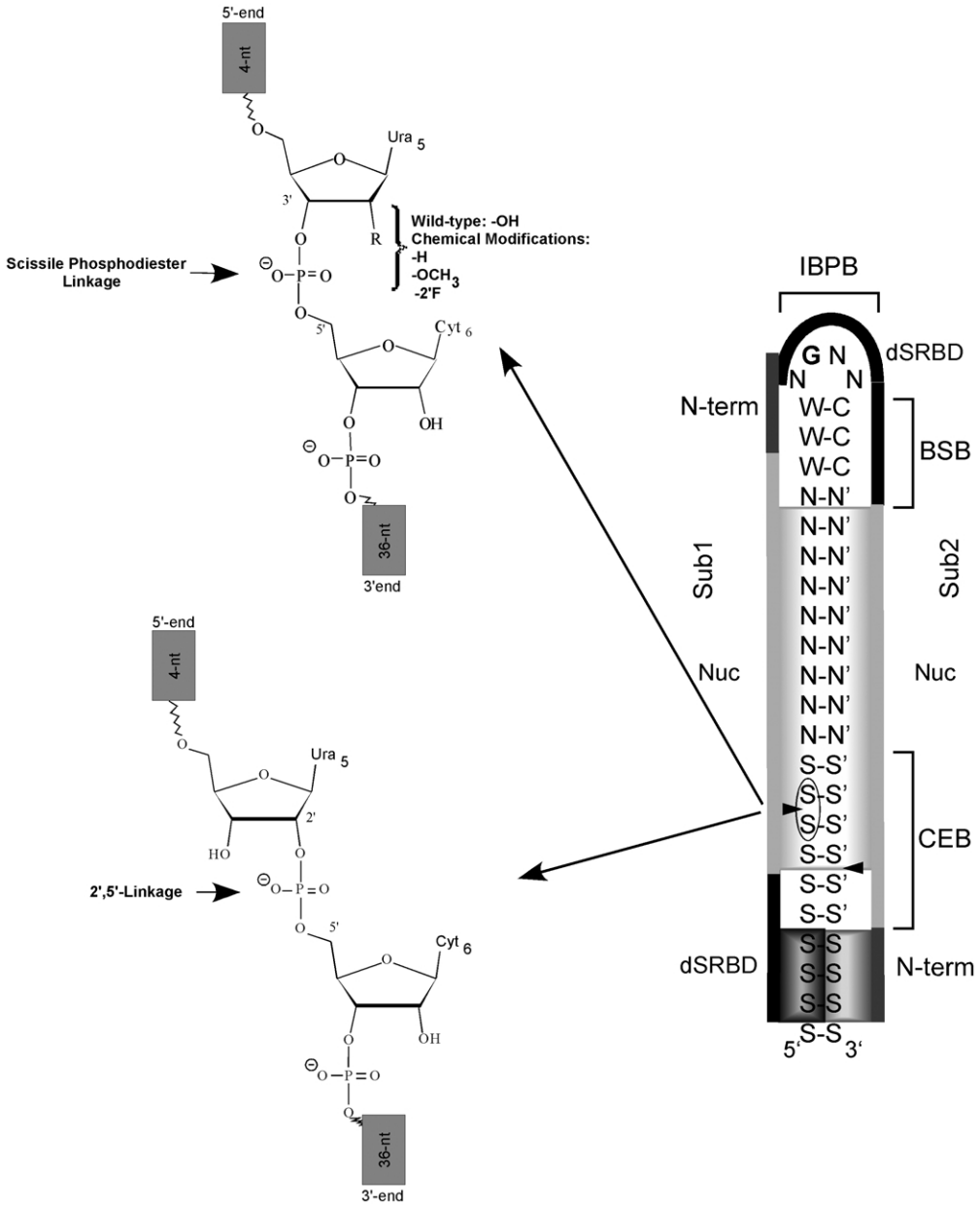

Figure 1. Schematic representation of a model RNA substrate illustrating the positioning of Rnt1p and the chemical modifications introduced in the course of this study. IBPB, BSB, and CEB indicate the nucleotide groups that influence Rnt1p initial binding and positioning, binding stability and cleavage efficiency.[22] The double-stranded RNA-binding domain (dsRBD) is illustrated in black, the nuclease domain (Nuc) in light gray and the N-terminal extension (N-term) in dark gray. The two subunits of the homodimer are labeled Sub1 and Sub2, respectively. N represents any nucleotide and N′ its complementary nucleotide including wobbles. W–C indicates positions where base-pairing is required. S indicates regions where base-pairing is not required. Arrowheads indicate the sites of cleavage. The chemical modifications introduced proximal to the scissile bond are indicated on the left.

conformation (*A*-form *versus B*-form) on Rnt1p binding and cleavage (Figure 3A). The purity and structural integrity of the oligomers were verified by matrix-assisted laser desorption/ionization time-of-flight (MALDI-TOF) mass spectrometry.

Rnt1p does not require the presence of a 2′ hydroxyl group near the cleavage site

As shown in Figure 2, the replacement of the uridine base 5′ to the scissile bond at position 15 from the tetraloop by 2′-deoxyuridine ($R_{19(dU)}LR_{19}$) did not block cleavage by Rnt1p. When compared with the all RNA substrate ($R_{19}LR_{19}$), the cleavage of $R_{19(dU)}LR_{19}$ was reduced by 34% in the presence of a low monovalent ion concentration (10 mM KCl), and by 64% in the presence of a physiological monovalent ion concentration (150 mM KCl) (data not shown). The introduction of 2′-*O*-methyluridine ($R_{19(2'OMe)}LR_{19}$) also permitted cleavage;

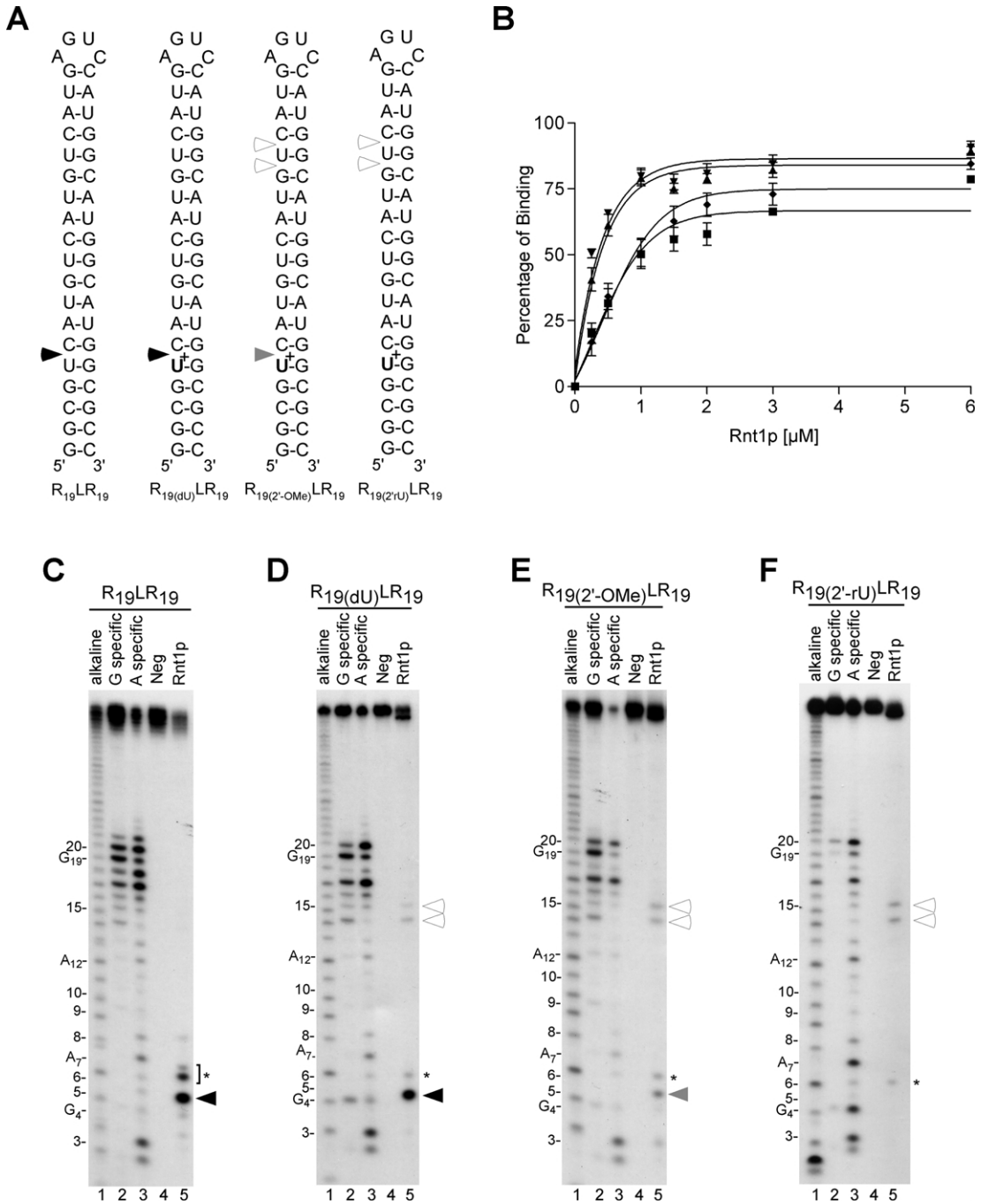

Figure 2. The 2′-hydroxyl group vicinal to the scissile phosphodiester linkage is not essential for Rnt1p cleavage. A, A model RNA substrate of 42 nucleotides specifically recognized by Rnt1p ($R_{19}LR_{19}$) was chemically modified at the cleavage site. The uracil at position 5 has been modified to deoxyuridine ($R_{19(dU)}LR_{19}$), 2′-OMe uridine ($R_{19(2'\text{-}OMe)}LR_{19}$), or the 3′,5′ linkage has been changed to 2′,5′ linkage ($R_{19(2'rU)}LR_{19}$). B, Quantitative analysis of Rnt1p binding to modified substrates. Increasing concentrations of Rnt1p were incubated with 2 fmol of $R_{19}LR_{19}$ (■), $R_{19(dU)}LR_{19}$ (▲),$R_{19(2'\text{-}OMe)}LR_{19}$ (▼), and $R_{19(2'rU)}LR_{19}$ (◆) and the binding percentage was plotted against the protein concentration (μM). The curve fits of data obtained from three independent experiments were calculated using Graph Pad Prism 3.0. The substrates $R_{19}LR_{19}$ (C), $R_{19(dU)}LR_{19}$ (D), $R_{19(2'\text{-}OMe)}LR_{19}$ (E) and $R_{19(2'rU)}LR_{19}$ (F) were 5′-end labeled and incubated under single turnover conditions in the absence (lanes 4) or the presence (lanes 5) of Rnt1p under low-salt concentration for 20 minutes at 30 °C. The cleavage products were fractionated by denaturing 20% PAGE. Each substrate was also subjected to alkaline hydrolysis (lane 1) and P_1 nuclease digestion in conditions that favors the cleavage 3′ to G (lanes 2) or 3′ to A (lanes 3). Positions of different nucleotides are indicated on the left. Black, gray and open arrows indicate strong, medium, and weak cleavages, respectively. The asterisks indicate products generated by Rnt1p cleavage at a non-canonical site 13 nt from the tetraloop. Cleavage at this site is observed in the presence of an excess of protein and low monovalent salt conditions.

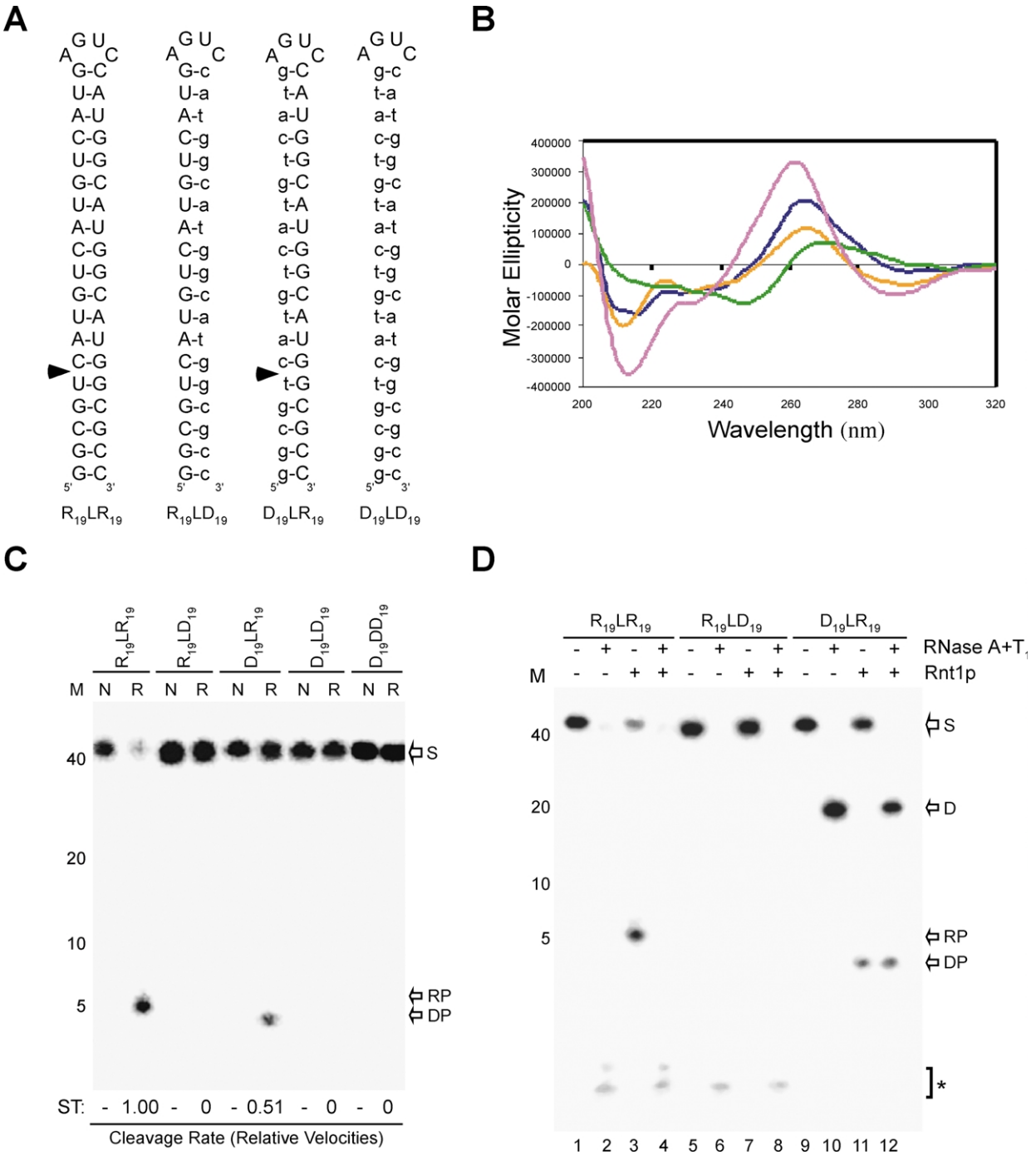

Figure 3. Rnt1p cleaves the DNA strand in a DNA/RNA hybrid capped with an AGUC RNA tetraloop. A, A schematic representation of the DNA/RNA chimeric hairpins subjected to Rnt1p cleavage. The chimeric substrates were based on the sequence of $R_{19}LR_{19}$, but were chemically synthesized with a DNA strand at the 3′ end ($R_{19}LD_{19}$), the 5′-end ($D_{19}LR_{19}$), or both the 3′- and 5′-ends ($D_{19}LD_{19}$) of the stem. $D_{19}DD_{19}$ was completely composed of DNA. The deoxyribonucleotides are indicated in small letters, while the ribonucleotides are indicated in capital letters. The arrowheads indicate the Rnt1p cleavage site. B, Circular dichroism spectra at 22 °C of representatives modified substrates are shown as follow: $R_{19}LR_{19}$ in blue, $D_{19}LR_{19}$ in orange, $D_{19}LD_{19}$ in green and $R_{19}LD_{19}$ in purple. Molar ellipticities were normalized to strand concentration. C, The different substrates were 5′-end labeled and incubated with excess recombinant Rnt1p in the presence of Mg^{2+} and low monovalent ion concentration. After incubation at 30 °C, the reaction products were loaded onto a denaturing 20% polyacrylamide gel and the bands visualized using Instant Imager. The RNA ladder is shown on the left. The substrate (S), RNA product (RP), and DNA product (DP) are indicated on the right. The all DNA substrate ($D_{19}DD_{19}$) is included as control on the right side of the gel. Rates under single turnover conditions (ST) are shown as fractional velocities relative to that of the parent substrate at bottom of the Figure. D, The 5′-end labeled substrates were subjected to RNase degradation either before or after Rnt1p cleavage reaction. Following the cleavage reactions, equal amounts of radioactivity were loaded onto a denaturing 20% polyacrylamide gel. The (+) and (−) signs represent the presence or absence of RNases and of Rnt1p in the reaction. The RNA ladder is indicated on the left of the gel, while the substrates (S), DNA strand (D), RNA product (RP) and DNA product (DP) are shown on the right. The asterisk represents free labeled phosphate.

however, the rate was reduced by 10–16% in the presence of both monovalent ion concentrations. At low monovalent ion concentrations, the cleavage of $R_{19(2'OMe)}LR_{19}$ resulted in the formation of products 5, 14 and 15 nucleotides (nt) long. The 5 nt product indicates cleavage at the predicted cleavage site, while the other two products correspond to non-canonical cleavage sites. Cleavage at non-canonical sites is similar to the star activity observed with DNA restriction enzymes,[3,22] and is induced in cleavage by Rnt1p and other RNase IIIs by the presence of low monovalent ion concentrations. The introduction of a single 2′,5′-phosphodiester linkage at position 15 ($R_{19(2'rU)}LR_{19}$) abolished cleavage at the canonical cleavage site; however, as observed with $R_{19(2'OMe)}LR_{19}$, cleavage at secondary sites were detected at low monovalent ion concentrations. Rnt1p products, which terminate with 3′-OH groups (Supplementary Figure 1), migrated more slowly than those generated by partial alkaline hydrolysis (Figure 2). We used nuclease P_1, which generates cleavage product similar to those predicted for Rnt1p, and becomes G-specific or A-preferential under certain cleavage conditions[28] to clearly map the site of the cleavage. We conclude that Rnt1p could cleave RNA substrates with 2′-deoxyuridine substitution near the cleavage site.

In order to ensure that any changes in the cleavage efficiency did not reflect either a global structural rearrangement or a change in stability, we examined the thermodynamic stability and conformation of all chemically modified substrates. Thermal denaturation experiments showed that all substrates exhibit single sigmoidal curves, indicating that they melt as a single entity (data not shown). The melting temperatures (T_m) were similar for all substrates (Table 1). Modest drops in the T_m were observed for the hairpins possessing a 2′,5′-phosphodiester linkage, as well as those with dU and 2′-OMe inserts. This may reflect a reduction in the base–base stacking interactions at the site of modification. Nevertheless, the substrates exhibited helical patterns typical of *A*-form RNA helices, as assessed by circular dichroism (data not shown). Furthermore, cleavage by bacterial RNase III, which takes place two nucleotides upstream of the Rnt1p cleavage site, was not affected by any of the introduced modifications, confirming the global helical stability of the hairpins (data not shown). Consistently, modifications near the cleavage site did not inhibit binding by Rnt1p (Figure 2B and Table 1). In fact, the apparent K'd of the poor substrate $R_{19(2'OMe)}LR_{19}$ was half that of the highly reactive $R_{19}LR_{19}$. The binding affinity of $R_{19(dU)}LR_{19}$ was also higher than that of $R_{19}LR_{19}$, while binding to $R_{19(2'rU)}LR_{19}$ was slightly lower. Thus, differences in the cleavage rate are not due to structural differences or binding anomalies. Together, these results show that the presence of the 2′-OH group is not essential at the site of cleavage, and suggest that cleavage by Rnt1p takes place by a mechanism similar to that of DNA restriction enzymes in which a metal ion is used to coordinate the attack of a nucleophilic water molecule.[20]

Table 1. Apparent dissociation constants, melting temperatures and percent hyperchromicities of chemically modified hairpin substrates under study

Entry	Designation	K'_d (μM)	T_m (°C)	%*H*
1	$R_{19}LR_{19}$	0.67	69.8	18.3
2	$R_{19(dU)}LR_{19}$	0.27	66.6	3.0
3	$R_{19(2'\text{-}OMe)}LR_{19}$	0.20	65.7	8.5
4	$R_{19(2'\text{-}rU)}LR_{19}$	0.95	62.9	14.6
5	$R_{19}LD_{19}$	2.20	50.6	11.7
6	$D_{19}LR_{19}$	2.40	60.8	7.6
7	$D_{19}LD_{19}$	0.96	53.7	13.6

UV thermal melting measurements were determined in 0.01 M Na_2HPO_4, 0.1 mM Na_2EDTA buffer, pH 7.00 ± 0.02 at an oligonucleotide concentration of 4.5 μM. Values represent the average of three independent measurements. Errors in the T_m values are ±0.5 °C. The melting curves show a single cooperative and completely reversible transition. The apparent dissociation constants (K'_d) were determined as described in the material and method section. Errors in the values of K'_d are within ±0.05 μM.

Rnt1p cleaves DNA in DNA/RNA hybrids

Escherichia coli RNase III cleaves RNA lacking a 2′-hydroxyl group at the cleavage site,[14] but cannot fully cleave either deoxyribose-substituted substrates or RNA/DNA hybrids.[11] This suggests that either the shape of the RNA helix, or the presence of certain 2′-hydroxyl groups, is important for RNase III interaction with its substrate. In order to assess the contributions of both the 2′-hydroxyl groups and the overall RNA *A*-form to Rnt1p substrate recognition, we examined the affinity of Rnt1p for different chimeric DNA/RNA substrates. Two hairpins, $R_{19}LD_{19}$ and $D_{19}LR_{19}$, were designed to form DNA/RNA "hybrid" helices, while $D_{19}LD_{19}$ and $R_{19}LR_{19}$ were designed to form *B*-form (dsDNA) and *A*-form (dsRNA) helices, respectively (Figure 3A). As shown in Figure 3B, the CD spectrum of $R_{19}LR_{19}$ very closely resembled that of an *A*-form RNA duplex, whereas the $D_{19}LD_{19}$ spectrum was typical of a *B*-form DNA duplex. Both the $D_{19}LR_{19}$ and the $R_{19}LD_{19}$ hybrids displayed similar "*A*-like" CD signatures, suggesting that they share the same overall helical conformation.

The different hairpins were incubated with Rnt1p in the absence of Mg^{2+}, and their binding affinities determined using gel mobility-shift assays. As expected, Rnt1p bound tightly to $R_{19}LR_{19}$ with an apparent K'_d of 0.67 μM (Table 1 and Supplementary Figure 2) but not to an all DNA substrate (data not shown). Surprisingly, $D_{19}LD_{19}$ bound to Rnt1p almost as efficiently as $R_{19}LR_{19}$ exhibiting an apparent K'_d of 0.96. This indicates that the ribonucleotide content of the tetraloop is essential and sufficient for binding within the context of a *B*-form DNA helix. Both

DNA/RNA hybrids ($D_{19}LR_{19}$ and $R_{19}LD_{19}$) bound Rnt1p three times less tightly than did $R_{19}LR_{19}$ (apparent K'_d of 2.4 μM and 2.2 μM, respectively). Interestingly, Rnt1p had higher affinity for hairpins with DNA stems than for hairpins with RNA/DNA or DNA/RNA hybrid stems. The results indicate that Rnt1p does not require the presence of either a 2′-hydroxyl group or an *A*-form RNA helix for binding. As shown in Figure 3C, Rnt1p cleaved the all RNA substrate $R_{19}LR_{19}$, as expected, while the all DNA substrate ($D_{19}DD_{19}$) resisted cleavage. The inability of Rnt1p to cleave an all DNA substrate is probably due to a combination of low binding affinity (data not shown) and failure to correctly position the substrate for cleavage that results from the perturbation in the loop structure.[23] Consistently, deoxyribose-substituted tetraloops bound poorly to Rnt1p (data not shown). Surprisingly, Rnt1p cleaved the DNA strand of the hybrid substrate $D_{19}LR_{19}$ indicating that Rnt1p cleavage is not RNA specific. As observed for the all RNA substrate, the cleavage of $D_{19}LR_{19}$ occurred 14 bp from the tetraloop, resulting in the release of a 5 nt DNA fragment. Rnt1p also cleaved the RNA strand of $D_{19}LR_{19}$ 16 bp from the tetraloop, as predicted (data not shown). Rnt1p bound, but did not cleave, both a hybrid containing a DNA strand at the 3′-end ($R_{19}LD_{19}$) and a complete DNA duplex ($D_{19}LD_{19}$). Cleavage was not observed even within the RNA strand of $R_{19}LD_{19}$, indicating that the presence of DNA at the 3′ end of the tetraloop not only blocks DNA based cleavage, but also interferes with cleavage on both sides of the stem. The inability of Rnt1p to cleave $R_{19}LD_{19}$ and $D_{19}LD_{19}$ is not a result of lower affinity (Table 1 and Supplementary Figure 2). Consistently, cleavage was not observed even when $R_{19}LD_{19}$ and $D_{19}LD_{19}$ were pre-bound to Rnt1p using the "in-the-gel" cleavage assay (data not shown).[27,29] This suggests that the presence of the ribonucleotides located at the 3′ end of the stem-loop are not essential for binding, but are required for cleavage.

In order to ensure that the observed cleavage of $D_{19}LR_{19}$ was occurring in the DNA strand, we digested all substrates with a mixture of RNases A and T_1[30,31] either directly or after cleavage with Rnt1p. As seen in Figure 3D, 5′-end labeled $R_{19}LR_{19}$ and the RNA portion of $R_{19}LD_{19}$ were completely degraded upon the addition of RNases A and T_1. As expected, the products released by the Rnt1p cleavage of $R_{19}LR_{19}$ were also completely degraded by the ribonuclease mixture. RNase treatment of $D_{19}LR_{19}$ resulted in a protected 19 nt fragment corresponding to the DNA component of the substrate. The products generated by the Rnt1p cleavage of $D_{19}LR_{19}$ resisted degradation by the mixture of RNases A and T_1. The RNases A and T_1 mixture cleaved, the RNA but not the DNA portion of the intact $D_{19}LR_{19}$. These experiments clearly show that Rnt1p can cleave DNA, and demonstrate that the hydrolysis of the scissile phosphodiester bond does not require the presence of a vicinal 2′-OH group. Rnt1p's capacity to cleave DNA illustrates the unexpected versatility of dsRBPs, and underlines the potential for new undiscovered substrates.

Helix homogeneity is essential for substrate recognition and cleavage by Rnt1p

Rnt1p displayed similar affinities for $R_{19}LD_{19}$ and $D_{19}LR_{19}$ hairpins (Table 1 and Supplementary Figure 2), but cleaved only the latter (Figure 3C). This suggests that the enzyme requires the presence of an RNA strand at the 3′-end of the tetraloop for the correct positioning of the substrate with respect to the catalytic core. Previous mutational,[22,24,25] biochemical,[21] and structural[23] analyses of Rnt1p substrates support this explanation and indicate that Rnt1p must contact the surface of the 3′-end of the strand adjacent to the tetraloop in order to direct cleavage.[25] The lower part of the stem is not essential for either binding or cleavage, and Rnt1p cleaves single-stranded RNAs attached to 9 bp hairpins indicating that the presence of ribonucleotides opposite to the cleavage site are not required for cleavage.[22,25] Thus, in theory, a DNA helix with an RNA tetraloop and 5 bp RNA stem should direct cleavage within the DNA duplex if the overall helical conformation of the substrate is tolerated by Rnt1p. In order to test this hypothesis we designed the chimeric hairpin $D_{14}R_5LR_5D_{14}$. This hairpin consists of a 5 bp RNA stem-loop (AGUC) linked to a 14 bp DNA segment (Figure 4A). Based on earlier studies,[32] this hairpin is expected to have a short *A*-form RNA helix followed by a *B*-form DNA helix. We also prepared the hairpin $D_{19}LR_5D_{14}$ in which the same 14 bp DNA segment is linked to a 5 bp DNA/RNA hybrid (Figure 4A). Interestingly, both substrates resisted cleavage (Figure 4B) and bound poorly to Rnt1p (Figure 4C). The low affinities of both $D_{19}LR_5D_{14}$ and $D_{14}R_5LR_5D_{14}$ for Rnt1p are not due to the substitution of any specific 2′-hydroxyl group, since a homogenous DNA helix capped with an AGUC tetraloop efficiently binds to Rnt1p (Table 1 and Supplementary Figure 2). Hairpins with 11 bp RNA helices, which normally bind to Rnt1p, lost their binding affinity when attached to a 5 bp *B*-form DNA helix (data not shown). These results clearly indicate that although Rnt1p could accommodate *B*-form, *A*-form, or *A*-like (hybrid) helices on their own, it does not tolerate a combination of these conformations (e.g. abrupt *A*/*B* junctions). However, the mechanism by which the ribonucleotides downstream of the tetraloop influence Rnt1p cleavage remains unclear.

Deoxyribonucleotide substitutions in Rnt1p reactivity epitopes inhibit binding and cleavage

Rnt1p recognizes its substrate using reactivity epitopes grouped into three regions: IBPB, BSB, and CEB (Figure 1). In order to determine the

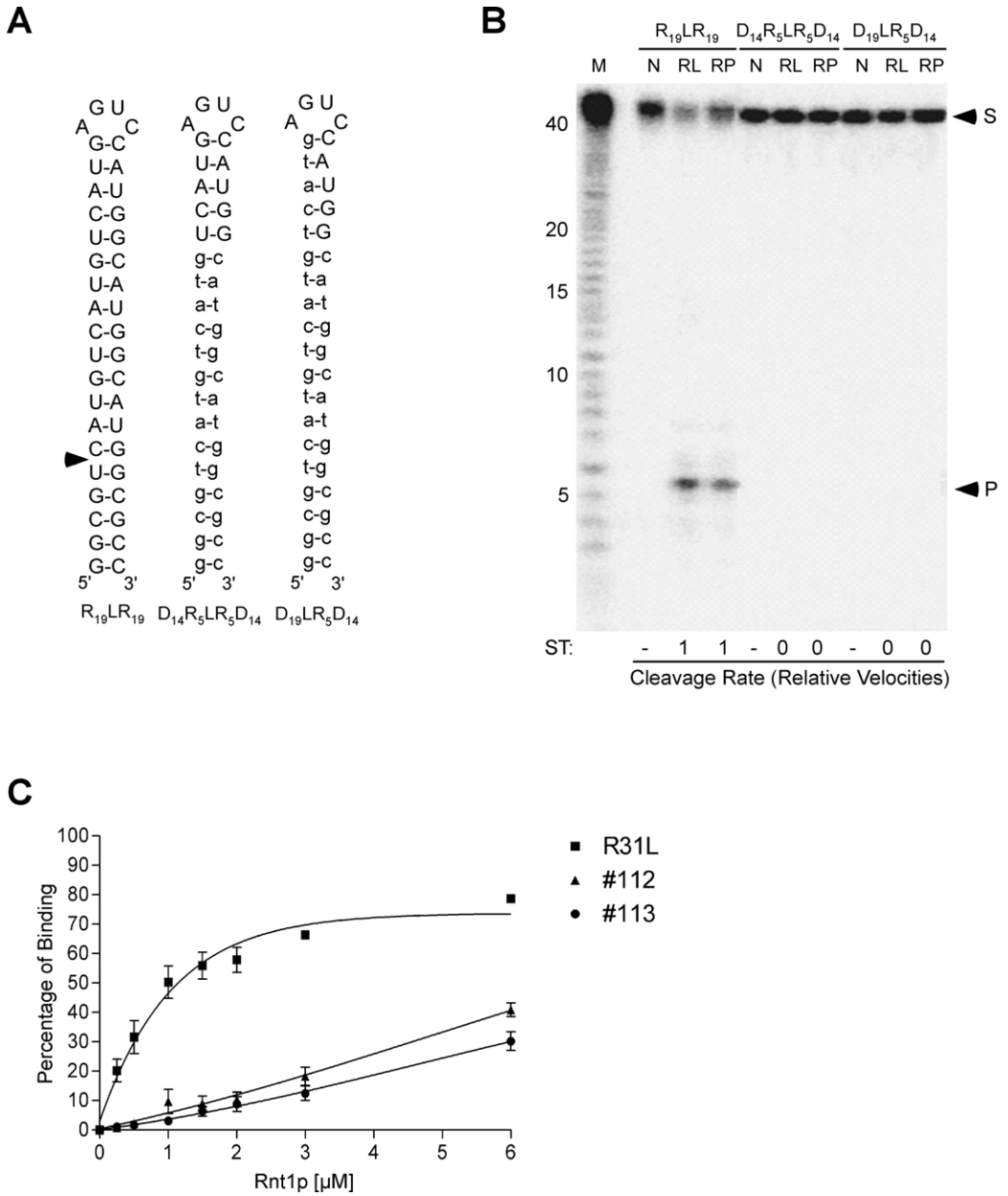

Figure 4. Helical heterogeneity blocks Rnt1p Cleavage. A, Hairpins based on the sequence of $R_{19}LR_{19}$ were synthesized with either a mixed RNA–DNA stem ($D_{14}R_5LR_5D_{14}$) or a mixed DNA–RNA/DNA stem ($D_{19}LR_5D_{14}$). The deoxyribonucleotides are indicated by small letters, while the ribonucleotides are indicated by capital letters. B, All hairpins were 5′-end labeled and incubated either alone (N), or with an excess of recombinant Rnt1p under either low-salt (RL) or physiological salt (RP) concentrations in the presence of Mg^{2+}. The reaction products were directly loaded onto a denaturing 20% polyacrylamide gel and visualized using an Instant Imager. The RNA marker produced by alkaline hydrolysis indicated on the left. The arrowhead indicates the Rnt1p cleavage site. Rates under single turnover conditions (ST) are shown as fractional velocities relative to that of the parent substrate at bottom of the Figure. C, Quantitative analysis of Rnt1p binding to modified substrates. Increasing concentrations of Rnt1p were incubated with 2 fmol of $R_{19}LR_{19}$ (■), $D_{14}R_5LR_5D_{14}$ (▲), and $D_{19}LR_5D_{14}$ (●) and the binding percentage was plotted against the protein concentration. The curve fits of data obtained from three independent experiments were calculated using Graph Pad Prism 3.0.

mechanism by which Rnt1p recognizes these reactivity epitopes, we tested the effects of deoxyribonucleotide substitutions within each group of nucleotides on binding and cleavage. All substitutions were performed using the hairpin $R_{16}LR_{16}$ (Figure 5A), which permits a single cleavage by Rnt1p.[22] Cleavage of each hairpin was performed either in the presence of an excess of substrate (8:1), or in the presence of an excess of enzyme (100:1). As expected, the all RNA substrate $R_{16}LR_{16}$ was 100% cleaved. The cleavage of the $D_{16}LR_{16}$ hybrid was reduced by 37% in the presence of an excess enzyme, and 93% in the presence of an excess substrate when compared to $R_{16}LR_{16}$

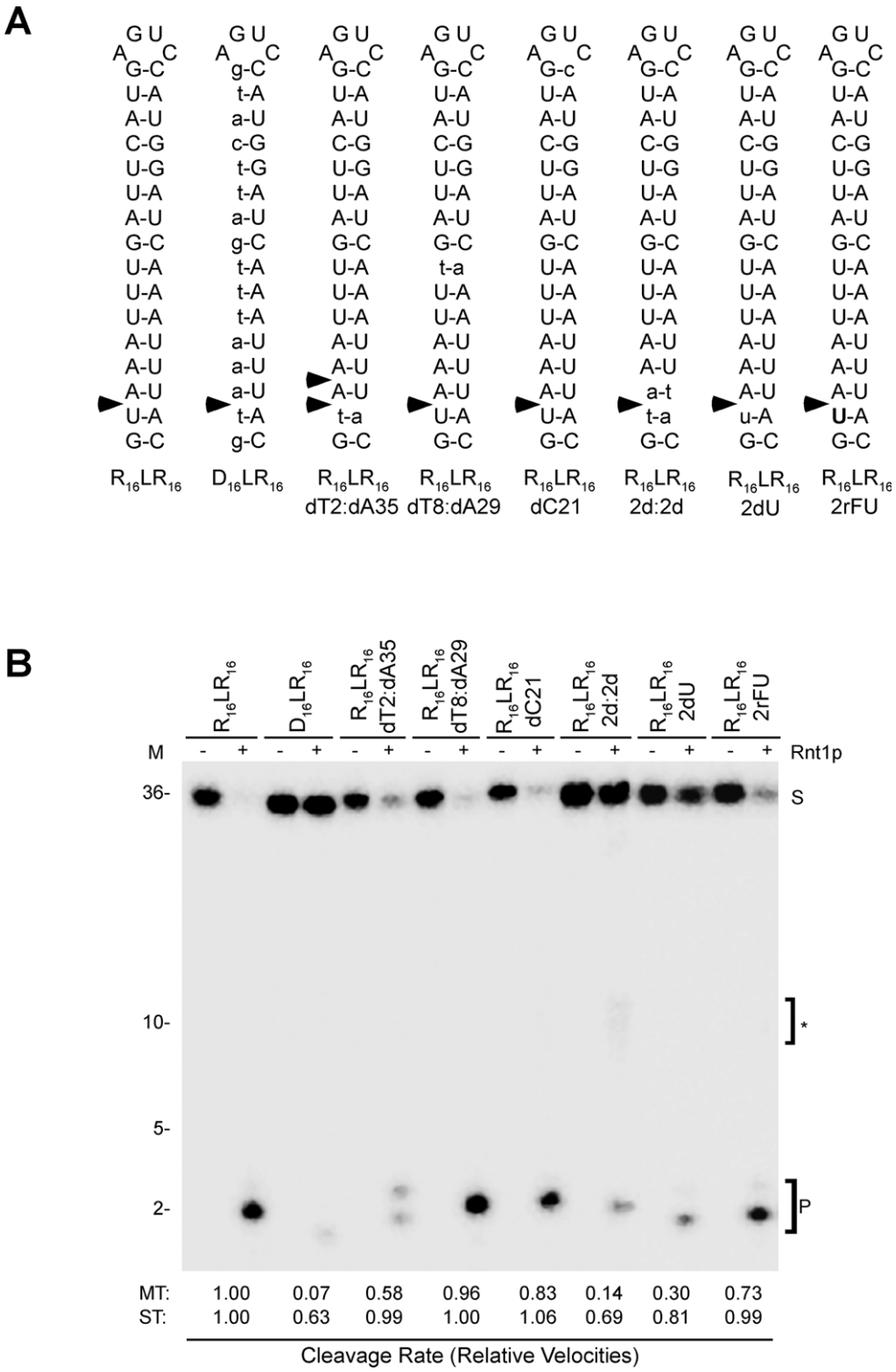

Figure 5. Deoxyribonucleotide substitutions of Rnt1p reactivity epitopes inhibit cleavage. A, Secondary structure representations of modified substrates relative to that of the RNA control ($R_{16}LR_{16}$). The black arrowheads represent cleavage by Rnt1p. B, The different substrates were 5′-end labeled and incubated in either the absence (−) or the presence (+) of recombinant Rnt1p for 20 minutes at 30 °C in reaction buffer. The cleavage products were directly loaded onto a denaturing 20% polyacrylamide gel and visualized using an Instant Imager. The cleavage reactions were carried out under either single (ST) using 20 nM of Rnt1p and 3 fmol of substrate or multiple (MT) turnover conditions (shown gel) using 80 nM of Rnt1p and 600 nM of substrate and the cleavage rates are relative to the parent substrate ($R_{16}LR_{16}$). The results shown are an average of three experiments. The alkaline marker is indicated on the left of the gel. The positions of the substrates (S) and products (P) are indicated on the right of the gel. The asterisk represents unspecific cleavage. The maximum error for the cleavage rate is ±0.03.

Table 2. Kinetic parameters of Rnt1p cleavage of chemically modified substrates

Substrate	K'_d (μM)	k_{cat} (min^{-1})	K_M (μM)	k_{cat}/K_M (l/mol min)
$R_{16}LR_{16}$	3.66	9.310	2.71	3.44×10^6
$D_{16}LR_{16}$	>6	0.058	3.80	1.51×10^4
$R_{16}LR_{16}$ dT2:dA35	2.45	0.053	0.11	0.49×10^6
$R_{16}LR_{16}$ dT8:dA29	3.96	3.380	1.10	3.08×10^6
$R_{16}LR_{16}$ dC21	>6	1.660	2.04	0.82×10^6
$R_{16}LR_{16}$ 2d:2d	2.55	0.078	0.51	0.15×10^6
$R_{16}LR_{16}$ 2dU	4.09	0.036	0.08	0.46×10^6
$R_{16}LR_{16}$ 2rFU	3.90	0.450	0.31	1.45×10^6

The K_M and k_{cat} values were determined by measuring the initial rate of production of the 2 nt cleavage product of the different substrates as a function of substrate concentration. The calculations were peformed using Prism 3.0 (GraphPad), and the apparent dissociation constants (K'_d) were determined as described in Materials and Methods. Errors in the values of the K'_d are within ±0.10 μM. The indicated values represent the average of four independent measurements using 5′-end labeled substrates. The maximum k_{cat} error limits are ±0.3 min^{-1} for $R_{16}LR_{16}$, $R_{16}LR_{16}$ dT8:dA29 and $R_{16}LR_{16}$ dC21, and ±0.006 min^{-1} for $D_{16}LR_{16}$, $R_{16}LR_{16}$ dT2:dA35, $R_{16}LR_{16}$ 2d:2d, $R_{16}LR_{16}$ 2dU, and $R_{16}LR_{16}$ 2rFU. The maximum K_M error limits are ± 0.03 μM for $R_{16}LR_{16}$ dT2:dA35, $R_{16}LR_{16}$ 2d:2d, $R_{16}LR_{16}$ 2dU and $R_{16}LR_{16}$ 2rFU, and ± 0.1 μM for $R_{16}LR_{16}$, $D_{16}LR_{16}$, $R_{16}LR_{16}$ dT8:dA29 and $R_{16}LR_{16}$ dC21.

(Figure 5B). Gel mobility-shift assays indicate that Rnt1p binds $D_{16}LR_{16}$ at least half as efficiently as $R_{16}LR_{16}$ (Table 2 and Supplementary Figure 3), which explains, in part, the reduced cleavage. This result is consistent with that obtained with the longer $D_{19}LR_{19}$ hybrid (Table 1). Substitution within the CEB changing the base-pair at the cleavage site into deoxyribonucleotides ($R_{16}LR_{16}$ dT2:dA35) did not affect the cleavage when the assay was performed in the presence of an excess enzyme. In contrast, the cleavage of $R_{16}LR_{16}$ dT2:dA35 was 42% less than that of $R_{16}LR_{16}$ and exhibited in a secondary cleavage site one nucleotide above the modified cleavage site when performed in excess substrate. Changing the four nucleotides that surround the cleavage site into deoxyribonucleotides ($R_{16}LR_{16}$2d:2d) further reduced the level of cleavage, especially in the presence of excess substrate. Introduction of a single deoxyribonucleotide at the cleavage site ($R_{16}LR_{16}$2dU) reduced cleavage by 70% and 19% in multiple turnover and single turnover conditions, respectively. This suggests that either difference in the structure of the deoxyribonucleotide sugar pucker perturbs the conformation of the cleavage site or that the 2′-OH group assists in the reaction. To differentiate between these two possibilities, we substituted the uridine residue at the cleavage site with 2′-fluorouridine, which maintains the same conformation as the native uridine unit (2′-OH sugar) and exhibits a similar pattern of electronegativity and bond polarity at C2′ ($R_{16}LR_{16}$2rFU). As shown in Figure 5, introduction of 2′-fluorouridine did not affect the cleavage in single turnover conditions, while moderately reducing cleavage in excess of RNA. These results indicate that the 2′-OH group plays a minor role in the cleavage reaction and suggest that the introduction of deoxyribonucleotides at the cleavage site may perturb the local conformation required for cleavage by Rnt1p.

Gel mobility-shift assay shows that the binding affinities were not affected by mutations in the CEB region (see Table 2). In contrast, a single deoxyribonucleotide substitution within the BSB ($R_{16}LR_{16}$dC21), which is required for binding,[22] significantly decreased the binding affinity (Table 2), while modestly reducing the cleavage rate in substrate excess (Figure 5B). In contrast, deoxyribonucleotide substitution in the middle of the RNA stem ($R_{16}LR_{16}$dT8:dA29) did not affect binding or cleavage by Rnt1p (Figure 5B). This indicates that the effect of substituting the reactivity epitopes is specific and not caused by reduction in the total number of 2′-hydroxyl groups or general perturbation of the stem structure. Consistently, the results shown in Figures 4 and 5 indicate that Rnt1p cleavage is reduced as the number of deoxyribonucleotide near the cleavage site increases and is completely blocked by six constitutive deoxyribonucleotides (data not shown). We conclude that although Rnt1p does not require a 2′-hydroxyl group for cleavage it does not tolerate a *B*-form DNA helix near the cleavage site.

Kinetics of Rnt1p cleavage of deoxyribonucleotide substituted substrates

To determine the kinetic parameters for Rnt1p processing under steady-state conditions, we measured the initial cleavage rates of all the substrates indicated in Figure 5A as a function of the concentration (data not shown and Table 2). The kinetic parameters of Rnt1p cleavage of the modified substrates indicated in Figure 5A are summarized in Table 2. The only $R_{16}LR_{16}$ variants that did not perturb the catalytic efficiency contained either 2rFU adjacent to the cleavage site ($R_{16}LR_{16}$ 2rFU) or a deoxyribonucleotide base-pair away from the cleavage site (dT8:dA29). In general, increasing the number of deoxyribonucleotides around the scissile bond reduced the catalytic efficiency. The most dramatic effect was observed with the DNA/RNA hybrid (D16LR16), which was cleaved at a much slower rate when compared with $R_{16}LR_{16}$. The K_M values of substrates harboring mutations in the helix away from the site of cleavage were similar to the RNA control, while mutations surrounding the scissile bond greatly affected the K_M values. The same was true for the k_{cat} values of substrates with deoxyribonucleotides near the scissile bond (Table 2). Globally, substitution in the middle of the helix or near the terminal tetraloop did not affect the rate of catalysis. The results suggest that although the 2′-hydroxyl group is not essential for cleavage it is required for optimal catalysis. It is difficult to ascertain the exact contribution of the 2′-hydroxyl group given the available kinetics parameters of

the cleavage of the $R_{16}LR_{16}$ 2rFU, which cannot discriminate between a subtle effect on catalysis, changes in the geometry of the catalytic core, or other defects like a slower product release.

Bacterial and fission yeast RNase III requires the presence of a dsRNA helix for cleavage

The capacity of Rnt1p to use a conserved NGNN tetraloop for binding and cleavage is unique among all studied members of the RNase III family that generally recognize the *A*-form of an RNA helix.[4] Rnt1p reliance on the tetraloop for substrate recognition explains it capacity to bind and cleave DNA/RNA hybrid, and suggests that other RNase III that fail to recognize the tetraloop will also fail to cleave duplexes that deviate from the *A*-form. In order to test this hypothesis, we examined the cleavage of $R_{16}LR_{16}$ and its deoxyribonucleotide-substituted derivatives (Figure 6B) by the fission yeast Pac1 and *E. coli* RNase III enzymes. $R_{16}LR_{16}$ was previously shown to be cleaved by both enzymes[33] and therefore permits the direct comparison between the three different RNase IIIs. Cleavage of each hairpin was performed either in the presence of an excess of either substrate (8:1) or enzyme (100:1). As shown in Figure 6B, $R_{16}LR_{16}$ was efficiently cleaved by both Pac1 and RNase III at their predicted cleavage sites. However, $D_{16}LR_{16}$ and $R_{16}LR_{16}$2d:2d were not cleaved by either Pac1 nor RNase III. *E. coli* RNase III cleavage of all the other modified substrates was reduced to different extents under both single and multiple turnover conditions (Figure 6). This result indicates that *E. coli* RNase III is sensitive to minor perturbations of the RNA *A*-form helix. However, we cannot exclude the possibility that *E. coli* RNase III directly interacts with all of the substituted 2′-hydroxyl groups. In general, Pac1 was less sensitive than *E. coli* RNase III and tolerated more substitutions outside of the cleavage site (Figure 6B). The results indicate that *E. coli* RNase III substrate recognition requires ribonucleotide-dependent features of the RNA helix, while Pac1 is affected only by perturbation near the cleavage site. Therefore, Rnt1p recognition of the DNA/RNA hybrid is probably a result of its unique tetraloop-dependent substrate recognition mechanism that alleviates the importance of the RNA specific helical feature. We conclude that the capacity to cleave DNA is restricted to the selected members of the RNase III family, like Rnt1p, that use a specific structural motif for cleavage.

DNA cleavage by yeast RNase III in cell extracts

The discovery that a member of the dsRBP family can bind to a DNA duplex capped at one end with an r(AGUC) loop is unexpected and points towards new biological activities for this group of enzymes. In order to determine whether or not the DNA cleavage is an intrinsic activity of wild-type Rnt1p, we examined the cleavage of DNA/RNA hybrids in yeast cell extracts. The yeast cell extracts were prepared following a procedure previously used to detect Rnt1p activity.[34] Cell extracts were prepared from wild-type cells either expressing Rnt1p or lacking the *RNT1* gene.[35] As shown in Figure 7A, the RNA hairpin ($R_{16}LR_{16}$) was stable in Δ*RNT1* extracts (ΔE), and no exonuclease activity was detected throughout the experiment. In sharp contrast, the RNA hairpin was cleaved at the predicted Rnt1p cleavage site when exposed to the wild-type cell extract (WE). The initial cleavage by Rnt1p was followed by exonuclease hydrolysis as previously observed for other Rnt1p substrates.[36] Incubation of the DNA/RNA hybrid ($D_{19}LR_{19}$) with Rnt1p *in vitro* resulted in cleavage of the 5′-DNA strand (Figure 3). In wild-type cell extracts, the hybrid was also cleaved to produce the Rnt1p-specific band and other bands that were not seen during cleavage with the recombinant Rnt1p. When this hybrid was treated with the Δ*RNT1* cell extract, the Rnt1p-specific band was absent, while other bands corresponding to Rnt1p-independent cleavage persisted. Rnt1p-independent endonucleolytic cleavages were observed in the RNA moiety of the substrate, and were likely introduced by RNase H, the only known DNA-dependent ribonuclease present in yeast cells.[37] The other Rnt1p independent cleavages occurred in the DNA strand and were likely mediated by single-stranded DNA endonucleases followed by exonucleolytic cleavage.[38,39] We conclude that natural Rnt1p enzyme can cleave DNA in an *in vivo*-like environment.

In order to further differentiate Rnt1p-dependent activities from other activities targeting DNA/RNA hybrids, such as helicases, exonucleases and metal-dependent ribonucleases, we performed the cleavage reactions in different conditions. As seen in Figure 7B, $R_{16}LR_{16}$ was cleaved in the wild-type extract, initially producing Rnt1p-dependent products that were subsequently trimmed, presumably by exonucleases. Consistent with this observation the addition of ssRNA stabilized the Rnt1p cleavage-dependent product and blocked the formation of the smaller RNA fragments observed in the untreated extracts (data not shown). The incubation of $D_{16}LR_{16}$ in cell extracts resulted in both Rnt1p-dependent and Rnt1p-independent cleavages that progressed with time (Figure 7A). All cleavage activities were blocked by the addition of EDTA to chelate the Mg^{2+} consistent with a metal-dependent cleavage mechanism. Pre-incubation of the extracts with hexokinase, which converts ATP to ADP[40], resulted in the same degradation pattern as observed with the untreated extracts (Figure 7B) indicating that ATP-dependent helicases were not involved. The addition of excess ssRNA or ssDNA did not alter the cleavage pattern, demonstrating that Rnt1p competes in cell extracts with many other nucleases for the DNA/RNA hybrid (Figure 7B). This is in marked contrast to what was observed for an RNA hairpin, which is very stable in the

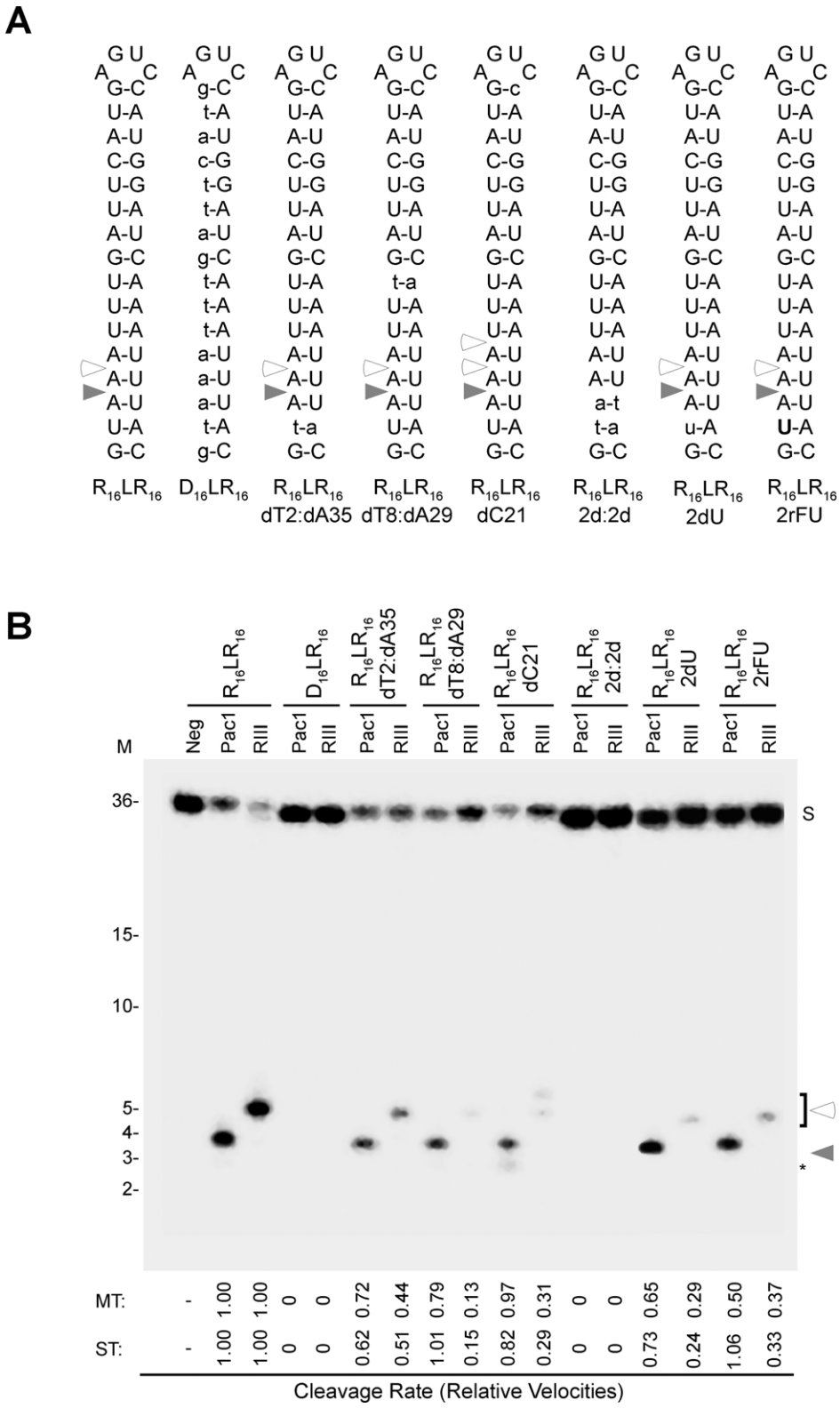

Figure 6. Bacterial and fission yeast RNase IIIs do not cleave DNA. A, Secondary structure representations of modified substrates relative to that of the RNA control ($R_{16}LR_{16}$). The gray and open arrowheads represent the Pac1 and *E. coli* cleavage sites, respectively. B, The substrates were 5′-end labeled and incubated either alone (Neg), or in the presence of either Pac1 or *E. coli* RNase III (RIII) under multiple turnover conditions. Following incubation, the reaction products were fractionated by denaturing 20% PAGE and visualized using an Instant Imager. The asterisk represents cleavage at non-canonical cleavage sites. The cleavage rates are presented as fractional velocities relative to that of the RNA control ($R_{16}LR_{16}$) when cleaved by either Pac1 or bacterial RNase III under single (ST) or multiple turnover (MT) conditions. The indicated values are the average of three experiments. The error margins for the cleavage rates are ± 0.03.

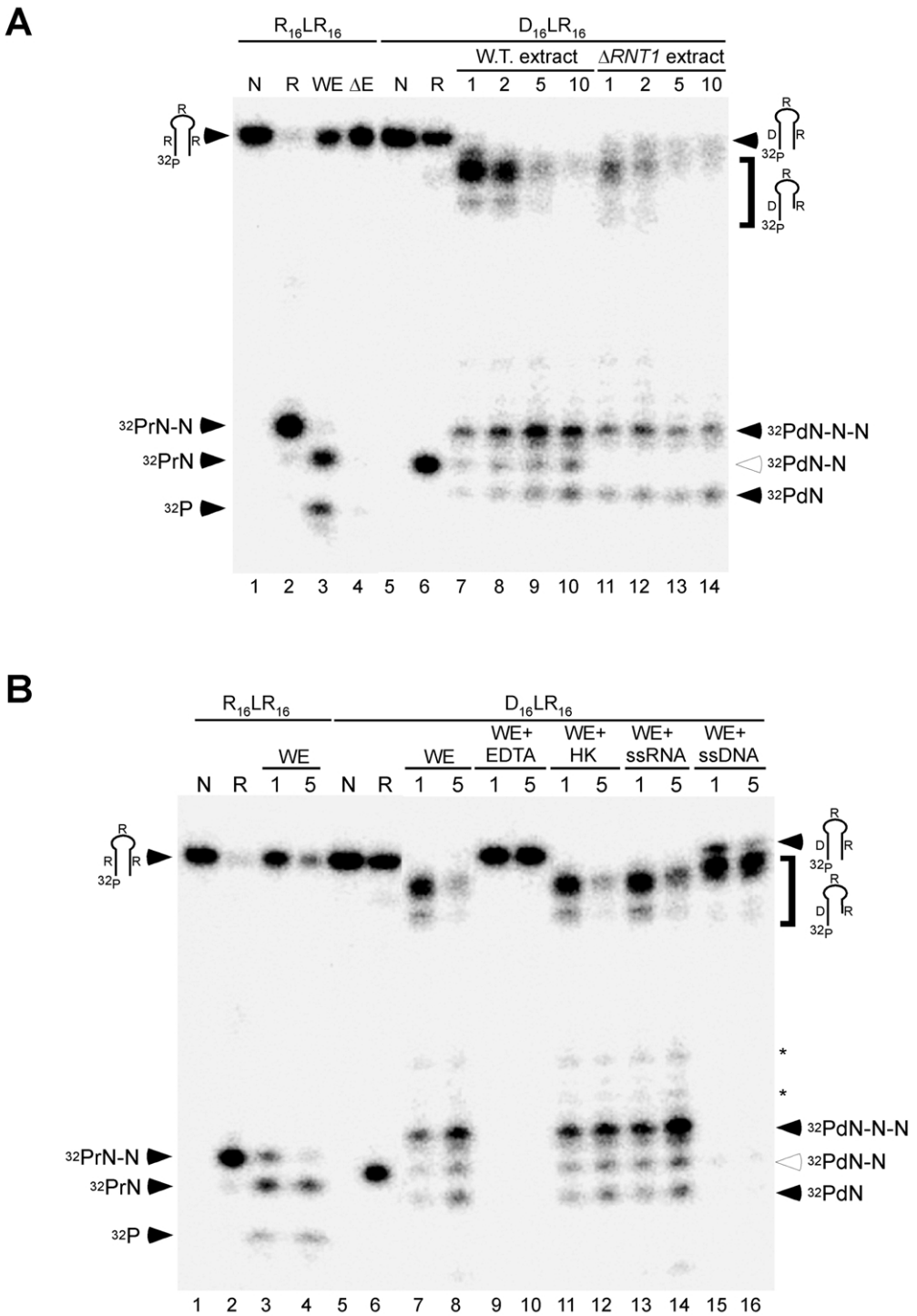

Figure 7. Yeast RNase III can specifically cleave the DNA moiety of a DNA/RNA hybrid in total yeast extracts. A, The snRNA U5-like substrate ($R_{16}LR_{16}$) and its counterpart hybrid ($D_{16}LR_{16}$) were 5′-end labeled and incubated either alone (N), with recombinant Rnt1p (R), or with wild-type (WE) or Δ*RNT1* (ΔE) yeast cell extracts for one minute, two minutes, five minutes, and ten minutes in the presence of Mg^{2+}. Following incubation at 30 °C, the RNA was phenol/chloroform-extracted. Equal amounts of radioactivity were loaded onto a denaturing 20% polyacrylamide gel and the products visualized using the Instant Imager. The structures corresponding to each band are indicated on the sides of the gel. The open arrowhead indicates Rnt1p-dependent DNA cleavage. B, Analysis of the DNA cleavage activity of Rnt1p in wild-type yeast extract. The substrates $R_{16}LR_{16}$ and $D_{16}LR_{16}$ were 5′-end labeled and incubated either alone (N), with excess recombinant Rnt1p (R), or with wild-type extract (WE). The reactions were performed as described for A, but were pretreated with EDTA, hexokinase (HK), single-stranded RNA (ssRNA) or single-stranded DNA (ssDNA).

absence of Rnt1p (Figure 7A). Together, this set of experiments shows that Rnt1p can identify and cleave DNA in a DNA/RNA hybrid, as a component of a whole cell extract, and effectively competes with other nucleases for the cleavage of the DNA/RNA hybrid.

Discussion

Here, we have shown that Rnt1p, a member of the dsRNA-specific RNase III family, is capable of both binding to a DNA helix and cleaving a DNA/RNA hybrid when it is capped with an RNA tetraloop. To our knowledge this is the first evidence of an RNA-dependent DNA cleavage activity for any protein enzyme. Recognition of the DNA/RNA hybrid is not a general feature of the RNase III family, since both bacterial and fission yeast RNase III failed to cleave helices that include a DNA strand. DNA binding and cleavage by Rnt1p indicates that the presence of dsRBD does not block interaction with the *B*-form DNA helix, and suggests that the substrate specificity of some members of the RNase III family might be wider than previously expected. Unlike RNase H,[41] Rnt1p supports catalysis in the absence of a 2′-OH group vicinal to the cleavage site, suggesting that hydrolysis occurs *via* a coordinated water molecule acting as the nucleophile, as is observed for DNA restriction enzymes.[20] *In vivo*, Rnt1p DNA cleavage could serve as a defense mechanism against viral infection, or could participate in programmed genomic deletions similar to the recently described dsRNA-dependent genome surveillance in ciliates.[42]

It is striking that Rnt1p, a member of the RNase III family exhibiting a canonical dsRNA-binding motif, fails to distinguish an RNA helix from a DNA one. The ability of dsRNA-specific ribonucleases to select their substrate is believed to be mediated by a dsRBD.[5,6] The dsRBD conserved αββββα structure[43,44] interacts *via* loops 2 and 4 with 2′-OH groups (minor groove) and the phosphodiester backbone (major groove), respectively, in order to differentiate RNA helices from DNA ones.[6,45] The results shown here suggest that either the structure of Rnt1p dsRBD evolved to fit the spacing of a DNA helix, or was otherwise changed to recognize the fold of the NGNN tetraloop instead of the helical shape of the RNA helix. The pattern of Rnt1p interactions with its RNA substrate, as deduced by hydroxyl radical footprinting,[33] chemical interference,[21] mutagenesis and chemical shift assays,[22] supports the latter hypothesis. Rnt1p interaction with the tetraloop is essential for cleavage, while the interaction with the RNA stem plays a more regulatory role that fine tunes the cleavage efficiency.[22] It is also possible that Rnt1p uses a different domain for substrate recognition, but several experiments show that the dsRBD by itself can accurately select Rnt1p substrates and that its deletion from the enzyme abolishes RNA binding.[27] In addition, the Rnt1p dsRBD binds RNA and DNA helices capped with NGNN tetraloops with similar efficiencies (B.L. & S.A.E., unpublished results); therefore, it is more likely that Rnt1p's capacity to bind DNA was introduced by changes in the structure of the dsRBD that permit tetraloop-dependent recognition. Indeed, comparison of Rnt1p with RNase III from other *Saccharomyces* species, bacteria and *Schizosaccharomyces pombe* reveals extensions in both the loops and the α helices lengths unique to *Saccharomyces* RNase III (Abou Elela, unpublished). Changes specific to Rnt1p in otherwise conserved motifs within the dsRBD (e.g. the GXXH motif in loop2) were also observed[22,24] and could perhaps explain its capacity to bind DNA helices. Mutations in Rnt1p are now required in order to identify the amino acid residues needed for NGNN tetraloop specificity and recognition of DNA helices. It will be interesting to determine whether the recognition of the tetraloop and the ability to bind DNA helices originate from the same amino acid residues.

The results presented here fit the current model for substrate recognition by Rnt1p. In this model Rnt1p binds as an antiparallel homodimer[19,33] in a process that is mediated by intermolecular interactions[27] between the two subunits (Figure 1). The dsRBD of one subunit recognizes the NGNN tetraloop and initiates the interaction with the substrate.[22,24] The recognition of the tetraloop is asymmetrical and supported by interaction between subunit 2 (see Figure 1) and the four nucleotides downstream of the tetraloop.[33] This conclusion is supported by the asymmetrical fold of the tetraloop,[23] as well as both chemical interference[21] and mutagenesis data.[22] Indeed, the presence of a DNA tetraloop blocks all binding and cleavage, and substituting the first ribonucleotide 3′ end of the tetraloop with deoxyribonucleotide reduces binding (Table 2). It is predicted that the N-terminal domain of subunit 1 positioned antiparallel to subunit 2 would be held in conformation by interaction with the dsRBD, and not through interaction with the RNA.[22,27] In agreement with this, changes of the RNA strand 5′-end of the tetraloop to DNA allows binding and cleavage, while changing the 3′-end strand blocks cleavage. The binding of the tetraloop and its adjacent sequence to the dsRBD is expected to guide the rest of the RNA stem into a tunnel, created by the interaction of the two nuclease domains, where cleavage occurs as described for *Aquifex aeolicus* RNase III.[19] The structure and conformation of the substrate sequence in the tunnel is critical for the stability of the functional enzyme–substrate complex. Changing the 3′,5′-phosphodiester bond at the cleavage site to the isomeric 2′, 5′-phosphodiester bond blocks cleavage without affecting the overall binding. Furthermore, introduction of two or four deoxyribonucleotides near the cleavage site decreases the K_M without affecting the catalytic efficiency.

Therefore, while the overall helical features of the *A*-form RNA helix are not essential for Rnt1p binding and cleavage, the conformation of the cleavage site does contribute to the cleavage efficiency.

It has been shown that Rnt1p binding does not necessarily lead to cleavage, and mutations that increase the substrate's affinity do not always enhance the cleavage rate.[22] Furthermore, Rnt1p binds differently to cleavable and resistant substrates, indicating the presence of productive and non-productive modes of binding.[33] The binding of Rnt1p to cleavable substrates (see the model in Figure 1) results in distinct sets of protein footprints as one nears the terminal NGNN tetraloop (IBPB and BSB), and another adjacent to the cleavage site (CEB), while binding to resistant substrate produces scattered footprints.[33] Interference with the Rnt1p-binding site adjacent to the tetraloop region (BSB) decreases binding stability, as judged by mobility-shift assays and consequently inhibits cleavage.[22] In contrast, interference with Rnt1p-binding site near the cleavage site decreases cleavage without affect binding.[22] In the course of this study we also observed that deoxyribonucleotides substitutions within the tetraloop region (BSB) significantly decreased the K'_d, without affecting the K_M, while substitutions near the cleavage site decreased the K_M without affecting the K'_d. This further supports the hypothesis that Rnt1p has two modes of binding, but only one active conformation, and is consistent with a two-step binding reaction.

Deletion of the ribose 2′-OH group at the cleavage site (rU to dU) does not block nucleophilic cleavage of the scissile phosphate group, but instead modestly reduces the cleavage by 40% as compared to cleavage of the unmodified substrate. Changes of the same ribonucleotide to 2′-fluorouridine had much less effect on catalysis, causing only a reduction in the turnover rate. This indicates that intramolecular assistance by the 2′-OH group is not essential, and suggests that a coordinated water molecule (or hydroxide ion) is the key nucleophilic species. Indeed, the proposed mechanism of bacterial RNase III hydrolysis involves the deprotonation of water, producing the hydroxide ion nucleophile, and protonation of the 3′ oxygen atom of the leaving group.[46] Rnt1p catalytic efficiency is not affected by the presence of deoxyribonucleotides near the cleavage site, but is greatly reduced by replacing one complete RNA strand with DNA (DNA–RNA–RNA).

Compared to other RNase III[14] and RNase P,[47,48] Rnt1p appears to be more tolerant to the absence of the 2′-hydroxyl group from the cleavage site. This is most likely due to the fact that, unlike the other enzymes, Rnt1p's primary-binding site (NGNN tetraloop) is situated away from the cleavage site and outside of the RNA helix. In summary, we propose that RNase III-mediated RNA cleavage involves an intermolecular hydrolysis reaction where the incoming nucleophile is a coordinated water molecule (or hydroxide ion) that attacks the scissile phosphodiester moiety without the assistance of the ribose 2′-hydroxyl group. The results presented here show that dsRBPs have much wider range of substrates than previously believed, and suggests that certain RNase III could function as an RNA-dependent DNase.

Materials and Methods

Oligomer preparation

RNA substrates $R_{19}LR_{19}$ and $R_{16}LR_{16}$ were enzymatically synthesized as described.[22] Other substrates were synthesized on an Applied Biosystems (381A) synthesizer using standard solid-phase phosphoramidite chemistry, or were synthesized by the University Core DNA Services (University of Calgary). The syntheses were performed on a 1 μmol scale using LCAA-controlled pore glass solid support (500 Å pore size) that was derivatized with the appropriate protected nucleoside.[49] Assembly of the sequences was carried out according to published protocols.[26,50] Monomer coupling times were ten minutes (RNA) and 120 seconds (DNA). Extended coupling times were used for riboguanosine phosphoramidite (15 minutes) and deoxyguanosine phosphoramidite (180 seconds). 4,5-Dicyanoimidazole (0.5 M) was used as the coupling reagent.[51] Following chain assembly, the column was extensively washed with anhydrous acetonitrile and dried by flushing with argon or helium. The CPG support was taken out of the column and treated with aqueous ammonia/ethanol (3:1 (v/v), 1 ml) for 48 hour at room temperature. After centrifugation, the supernatant was collected and the solid support was washed with ethanol (3 × 1 ml). The supernatant and ethanol washings were combined and cooled to −20 °C for at least one hour before they were centrifuged and evaporated to dryness. The 2′-t-butyldimethylsilyl protecting groups, were removed by targeting the pellet with neat $NEt_3{\cdot}3HF$ (100 μl) at room temperature for 48 hours (only RNA-containing oligomers).[52] The reaction was quenched by the addition of deionized, double distilled water. The resulting solution was lyophilized to dryness under vacuum (Savant Industries Speed-Vac®), and subsequently purified by denaturing polyacrylamide gel electrophoresis (25% (w/v) acrylamide, 5% (w/v) bis-acrylamide and 7 M urea in water). The purified oligomers were desalted on a Sephadex® column[26] and subsequently evaporated to dryness under vacuum. Their structures were confirmed by MALDI-TOF mass spectrometry (data not shown).

UV-melting studies

UV thermal denaturation curves were obtained on a Varian CARY 1 UV–VIS spectrophotometer equipped with a multi-cell holder and a Peltier temperature-controller. Data acquisition and analysis were performed using Cary WinUV version 2 software (Varian Ltd). All thermal measurements were conducted in 0.01 M Na_2HPO_4, 0.1 mM Na_2EDTA buffer, pH 7.00 ± 0.02. Absorbance *versus* temperature spectra were collected at 265 nm over a range from 5 °C to 90 °C with 0.1 deg. C increments and a heating rate of 0.5 deg. C/min. Samples (~4.5 μM) were annealed by heating rapidly to 95 °C for 10–15 minutes, followed by slow cooling to

room temperature, and finally by incubation at 5 °C for 48 hours. Before data acquisition, oligonucleotides were degassed in an ultrasound bath for three minutes, and then equilibrated at 5 °C for at least ten minutes prior to the melting run. Melting temperatures were calculated according to the base-line method.[50] Single-strand molar extinction coefficients were calculated from those of the mononucleotides and dinucleotides using the nearest-neighbor approximation method.[53] 2′,5′-RNA was assumed to have the same molar extinction coefficient as RNA. Single-strand concentration was determined from UV absorbance at high temperature. The percentage hypochromicity (%*H*) was calculated from UV absorbances of the formed complex (A_f) and fully denatured species (A_0) using the following equation: $\%H = (A_f - A_0)/A_f$.

Circular dichroism studies

CD spectra were acquired on a JASCO J710 spectropolarimeter equipped with an external constant-temperature NESLAB RTE-111 circulating bath for temperature control. Fused quartz cells (Hellma, 165-QS) were used. Each spectrum represents the average of five independent 220–340 nm scans obtained at a rate of 0.5 nm/minute (bandwidth: 1 nm; sampling wavelength: 0.2 nm). The buffer used was 0.01 M Na_2HPO_4, 0.1 mM Na_2EDTA, pH 7.00 ± 0.02. The data were processed on a PC computer using Windows™ based software supplied by the manufacturer (JASCO, Inc.). The obtained CD spectra were normalized by subtraction of the background scan with buffer. Taking the known oligonucleotide concentration into account, the normalized spectra were converted to molar ellipticities.

Enzyme preparations

Recombinant Rnt1p was over-expressed in bacteria and purified as described.[29] Recombinant Pac1 was produced from the pQE32/Pac1 plasmid generated by cloning a PCR fragment amplified using the primers 5′-CTACCACTGAGTATGGGACGG-3′ and 5′-GCTTGACT CGAGTCTTAAACCCAG-3′ and pIRT31-Pac1 as a template[54] into the XhoI site of pQE32 (Qiagen Inc., Mississauga, Ont., Canada). pQE32/Pac1 was transformed into *E. coli* M15-pREP4 (Qiagen Inc., Mississauga, Ont., Canada) and Pac1 prepared using Rnt1p purification scheme.[29] Bacterial RNase III purification was performed essentially as described.[55]

Substrate preparation and *in vitro* cleavage assays

The substrates were 5′-end radiolabeled using [γ-^{32}P]ATP and T4 PNK (New England Biolabs) followed by gel purification as described.[22] For the *in vitro* cleavage assay, varying amount of substrates (indicated in the description of each experiment) were incubated in the presence of either 0.2–1.6 pmol of Rnt1p or 0.2 pmol of *E. coli* RNase III, for 20 minutes at 30 °C in 20 μl of reaction buffer.[23] Pac1 cleavage was performed by incubating the varying amount of substrates (indicated in the description of each experiment) with 1.6 pmol of enzyme for 20 minutes at 30 °C in 20 μl of reaction buffer (30 mM Ches (pH 8.5), 1 mM DTT, 5 mM $MgCl_2$, 10 mM KCl, and 0.1 mg/ml of BSA). The kinetic parameter shown in Table 2 were obtained using 20 nM or 320 nM Rnt1p and a 5′-end labeled substrate concentration higher than 50 nM. The cleavage rates were measured at 30 °C. The RNA ladders used as a marker was generated by either alkaline hydrolysis or nuclease P_1 digestion as described before.[22] RNase A and T_1 treatment was carried in 1X OPA buffer (Amersham Biosciences, Baie d'Urfé, QC, Canada) using 3 μg of RNase A and 30 units of RNase T_1 and incubating for 15 minutes at 37 °C. Cleavage in yeast cell extract was preformed at 30 °C with 30% of extract in 20 μl of Rnt1p cleavage buffer.[29] The reactions were stopped by phenol/chloroform-extraction and loaded onto denaturing 20% polyacrylamide gels. All experiments were repeated a minimum of three times. All kinetic calculations used here were done using the GraphPad Prism 3.0 program (GraphPad Software, CA).

Gel mobility-shift assay

RNA-binding assays were performed using 2 fmol of 5′-end labeled RNA in 20 μl of binding buffer (20% (v/v) glycerol, 30 mM Tris (pH 7.5), 150 mM KCl, 5 mM spermidine, 0.1 mM DTT, and 0.1 mM EDTA (pH 7.5)) for ten minutes on ice.[29] For each experiment, the amount of protein used ranged between 0.25 and 6 μ mol. The reactions were fractionated on non-denaturing 4% polyacrylamide gels using 0.5 V/cm^2 at 4 °C. All calculations and curves used here were done using the Graph Pad Prism 3.0 program (GraphPad Software, CA). Experiments were repeated four times.

Yeast extracts preparation and cleavage

Yeast extracts were prepared as described earlier[56] with slight modifications. Three liters of yeast culture (W303 or Δ*RNT1* strain) were grown to 0.8 A_{600} at 26 °C in YEPD. Cells were harvested by centrifugation, washed, and resuspended in 0.4 times the cell pellet's volume of AGK buffer (10 mM Hepes (pH 7.9), 1.5 mM $MgCl_2$, 200 mM KCl, 10% glycerol, 1 mM PMSF, 1 mM benzamidine, 1 μg/ml of leupeptin, 1 μg/ml of aprotinin, 1 μg/ml of pepstatin A, and 1 μg/ml of antipain). Following cell lysis in liquid nitrogen, the frozen powder was transferred to a centrifuge tube and centrifuged at 18,900 *g* for 30 minutes. The supernatant was then centrifuged at 94,000 *g* for 30 minutes and dialyzed for three hours against 2 l of dialysis buffer (20 mM Hepes (pH 7.0), 0.2 mM EDTA, 0.5 mM DTT, 50 mM KCl, and 20% glycerol). Finally, the extract was centrifuged at 18,900 *g* for 20 minutes and the supernatant was stored at −80 °C.

Acknowledgements

We thank Stephanie Larose for help with the preparation of the yeast cell extract. We thank Jean-Pierre Perreault for reading the manuscript and stimulating discussion. We acknowledge the financial support of the Canadian Institute for Health Research (CIHR; grant no. MOP-14305 to S.A.) and the Natural Science and Engineering Council of Canada (NSERC; grant to M.J.D). Support for the RNA group core is provided by CIHR. S. A. is a Chercheur-Boursier Junior II of the Fonds de la Recherche en Santé du Québec. B.L. was supported by a grant from the

FRSQ-FCAR. R.N.H. acknowledges support from NSERC and FCAR scholarships.

References

1. Bernstein, E., Denli, A. M. & Hannon, G. J. (2001). The rest is silence. *RNA*, **7**, 1509–1521.
2. Williams, B. R. (1999). PKR; a sentinel kinase for cellular stress. *Oncogene*, **18**, 6112–6120.
3. Nicholson, A. W. (1996). Structure, reactivity, and biology of double-stranded RNA. *Prog. Nucl. Acid Res. Mol. Biol.* **52**, 1–65.
4. Lamontagne, B., Larose, S., Boulanger, J. & Elela, S. A. (2001). The RNase III family: a conserved structure and expanding functions in eukaryotic dsRNA metabolism. *Curr. Issues Mol. Biol.* **3**, 71–78.
5. Johnston, D., St, Brown, N. H., Gall, J. G. & Jantsch, M. (1992). A conserved double-stranded RNA-binding domain. *Proc. Natl Acad. Sci. USA*, **89**, 10979–10983.
6. Ramos, A., Grunert, S., Adams, J., Micklem, D. R., Proctor, M. R., Freund, S. *et al.* (2000). RNA recognition by a Staufen double-stranded RNA-binding domain. *EMBO. J.* **19**, 997–1009.
7. Saunders, L. R. & Barber, G. N. (2003). The dsRNA binding protein family: critical roles, diverse cellular functions. *FASEB J.* **17**, 961–983.
8. Fierro-Monti, I. & Mathews, M. B. (2000). Proteins binding to duplexed RNA: one motif, multiple functions. *Trends Biochem. Sci.* **25**, 241–246.
9. Conrad, C. & Rauhut, R. (2002). Ribonuclease III new sense from nuisance. *Int. J. Biochem. Cell Biol.* **34**, 116–129.
10. Zhang, K. & Nicholson, A. W. (1997). Regulation of ribonuclease III processing by double-helical sequence antideterminants. *Proc. Natl Acad. Sci. USA*, **94**, 13437–13441.
11. Robertson, H. D. & Dunn, J. J. (1975). Ribonucleic acid processing activity of *Escherichia coli* ribonuclease III. *J. Biol. Chem.* **250**, 3050–3056.
12. Robertson, H. D. (1967). A nuclease specific for double-stranded RNA. *Virology*, **12**, 718.
13. Crouch, R. J. (1974). Ribonuclease III does not degrade deoxyribonucleic acid–ribonucleic acid hybrids. *J. Biol. Chem.* **249**, 1314–1316.
14. Nicholson, A. W. (1992). Accurate enzymatic cleavage *in vitro* of a 2′-deoxyribose-substituted ribonuclease III processing signal. *Biochim. Biophys. Acta*, **1129**, 318–322.
15. Steitz, T. A. & Steitz, J. A. (1993). A general two-metal-ion mechanism for catalytic RNA. *Proc. Natl Acad. Sci. USA*, **90**, 6498–6502.
16. Li, H. L., Chelladurai, B. S., Zhang, K. & Nicholson, A. W. (1993). Ribonuclease III cleavage of a bacteriophage T7 processing signal. Divalent cation specificity, and specific anion effects. *Nucl. Acids Res.* **21**, 1919–1925.
17. Schweitz, H. & Ebel, J. P. (1971). A study of the mechanism of action of *E. coli* ribonuclease 3. *Biochimie*, **53**, 585–593.
18. Rotondo, G. & Frendewey, D. (1996). Purification and characterization of the Pac1 ribonuclease of *Schizosaccharomyces pombe*. *Nucl. Acids Res.* **24**, 2377–2386.
19. Blaszczyk, J., Tropea, J. E., Bubunenko, M., Routzahn, K. M., Waugh, D. S., Court, D. L. & Ji, X. (2001). Crystallographic and modeling studies of RNase III suggest a mechanism for double-stranded RNA cleavage. *Structure (Camb)*, **9**, 1225–1236.
20. Pingoud, A. & Jeltsch, A. (2001). Structure and function of type II restriction endonucleases. *Nucl. Acids Res.* **29**, 3705–3727.
21. Chanfreau, G., Buckle, M. & Jacquier, A. (2000). Recognition of a conserved class of RNA tetraloops by *Saccharomyces cerevisiae* RNase III. *Proc. Natl Acad. Sci. USA*, **97**, 3142–3147.
22. Lamontagne, B., Ghazal, G., Lebars, I., Yoshizawa, S., Fourmy, D. & Abou Elela, S. (2003). Sequence dependence of substrate recognition and cleavage by yeast RNase III. *J. Mol. Biol.* **327**, 985–1000.
23. Lebars, I., Lamontagne, B., Yoshizawa, S., Abou Elela, S. & Fourmy, D. (2001). Solution structure of conserved AGNN tetraloops: insights into Rnt1p RNA processing. *EMBO. J.* **20**, 7250–7258.
24. Nagel, R. & Ares, M., Jr (2000). Substrate recognition by a eukaryotic RNase III: the double-stranded RNA-binding domain of Rnt1p selectively binds RNA containing a 5′-AGNN-3′ tetraloop. *RNA*, **6**, 1142–1156.
25. Abou Elela, S. & Ares, M. (1998). Depletion of yeast RNase III blocks correct U2 3′ end formation and results in polyadenylated but functional U2 snRNA. *EMBO J.* **17**, 3738–3746.
26. Damha, M. J. & Ogilvie, K. K. (1993). Oligoribonucleotide synthesis. The silyl-phosphoramidite method. *Methods Mol. Biol.* **20**, 81–114.
27. Lamontagne, B., Tremblay, A. & Abou Elela, S. (2000). The N-terminal domain that distinguishes yeast from bacterial RNase III contains a dimerization signal required for efficient double-stranded RNA cleavage. *Mol. Cell Biol.* **20**, 1104–1115.
28. Cruz-Reyes, J., Piller, K. J., Rusche, L. N., Mukherjee, M. & Sollner-Webb, B. (1998). Unexpected electrophoretic migration of RNA with different 3′ termini causes an RNA sizing ambiguity that can be resolved using nuclease P1-generated sequencing ladders. *Biochemistry*, **37**, 6059–6064.
29. Lamontagne, B. & Abou Elela, S. (2001). Purification and characterization of *Saccharomyces cerevisiae* Rnt1p nuclease. In *Methods in Enzymology* (Nicholllson, A. W., ed.), pp. 342, Academic Press, San Diego, CA.
30. Yakovlev, G. I., Sorrentino, S., Moiseyev, G. P. & Libonati, M. (1995). Double-stranded RNA the variables controlling its degradation by RNases. *Nucl. Acids Symp. ser.*, 106–108.
31. Both, V., Moiseyev, G. P. & Sevcik, J. (1991). Specificity of guanylic RNases to polynucleotide substrates. *Biochem. Biophys. Res. Commun.* **177**, 630–635.
32. Chou, S. H., Flynn, P., Wang, A. & Reid, B. (1991). High-resolution NMR studies of chimeric DNA–RNA–DNA duplexes, heteronomous base pairing, and continuous base stacking at junctions. *Biochemistry*, **30**, 5248–5257.
33. Lamontagne, B. & Abou Elela, S. (2004). Evaluation of the RNA determinants for bacterial and yeast RNase III binding and cleavage. *J. Biol. Chem.* **279**, 2231–2241.
34. Chanfreau, G., Abou Elela, S., Ares, M., Jr & Guthrie, C. (1997). Alternative 3′-end processing of U5 snRNA by RNase III. *Genes. Dev.* **11**, 2741–2751.
35. Chanfreau, G., Rotondo, G., Legrain, P. & Jacquier, A. (1998). Processing of a dicistronic small nucleolar RNA precursor by the RNA endonuclease Rnt1. *EMBO J.* **17**, 3726–3737.
36. Allmang, C., Kufel, J., Chanfreau, G., Mitchell, P.,

Petfalski, E. & Tollervey, D. (1999). Functions of the exosome in rRNA, snoRNA and snRNA synthesis. *EMBO J.* **18**, 5399–5410.
37. Wintersberger, U. & Frank, P. (2001). Ribonucleases H of the budding yeast, *Saccharomyces cerevisiae*. *Methods Enzymol.* **341**, 414–429.
38. Moreau, S., Morgan, E. A. & Symington, L. S. (2001). Overlapping functions of the *Saccharomyces cerevisiae* Mre11. Exo1 and Rad27 nucleases in DNA metabolism. *Genetics*, **159**, 1423–1433.
39. Huang, K. N. & Symington, L. S. (1993). A 5′-3′ exonuclease from *Saccharomyces cerevisiae* is required for *in vitro* recombination between linear DNA molecules with overlapping homology. *Mol. Cell. Biol.* **13**, 3125–3134.
40. Zamore, P. D., Tuschl, T., Sharp, P. A. & Bartel, D. P. (2000). RNAi: double-stranded RNA directs the ATP-dependent cleavage of mRNA at 21 to 23 nucleotide intervals. *Cell*, **101**, 25–33.
41. Yazbeck, D. R., Min, K. L. & Damha, M. J. (2002). Molecular requirements for degradation of a modified sense RNA strand by *Escherichia coli* ribonuclease H1. *Nucl. Acids Res.* **30**, 3015–3025.
42. Yao, M. C., Fuller, P. & Xiaohui, X. (2003). Programmed DNA deletion as an RNA-guided system of genome defense. *Science*, **300**, 1581–1584.
43. Kharrat, A., Macias, M. J., Gibson, T. J., Nilges, M. & Pastore, A. (1995). Structure of the dsRNA binding domain of *E. coli* RNase III. *EMBO J.* **14**, 3572–3584.
44. Nanduri, S., Carpick, B. W., Yang, Y., Williams, B. R. & Qin, J. (1998). Structure of the double-stranded RNA-binding domain of the protein kinase PKR reveals the molecular basis of its dsRNA-mediated activation. *EMBO J.* **17**, 5458–5465.
45. Ryter, J. M. & Schultz, S. C. (1998). Molecular basis of double-stranded RNA-protein interactions: structure of a dsRNA-binding domain complexed with dsRNA. *EMBO J.* **17**, 7505–7513.
46. Campbell, F. E., Jr, Cassano, A. G., Anderson, V. E. & Harris, M. E. (2002). Pre-steady-state and stopped-flow fluorescence analysis of *Escherichia coli* ribonuclease III: insights into mechanism and conformational changes associated with binding and catalysis. *J. Mol. Biol.* **317**, 21–40.
47. Perreault, J. P. & Altman, S. (1992). Important 2′-hydroxyl groups in model substrates for M1 RNA, the catalytic RNA subunit of RNase P from *Escherichia coli*. *J. Mol. Biol.* **226**, 399–409.
48. Forster, A. C. & Altman, S. (1990). External guide sequences for an RNA enzyme. *Science*, **249**, 783–786.
49. Pon, R. T., Yu, S. & Sanghvi, Y. S. (1999). Rapid esterification of nucleosides to solid-phase supports for oligonucleotide synthesis using uronium and phosphonium coupling reagents. *Bioconjug. Chem.* **10**, 1051–1057.
50. Hannoush, R. N. & Damha, M. J. (2001). Remarkable stability of hairpins containing 2′,5′-linked RNA loops. *J. Am. Chem. Soc.* **123**, 12368–12374.
51. Jellinek, D., Green, L. S., Bell, C., Lynott, C. K., Gill, N., Vargeese, C. *et al.* (1995). Potent 2′-amino-2′-deoxypyrimidine RNA inhibitors of basic fibroblast growth factor. *Biochemistry*, **34**, 11363–11372.
52. Gasparutto, D., Livache, T., Bazin, H., Duplaa, A. M., Guy, A., Khorlin, A. *et al.* (1992). Chemical synthesis of a biologically active natural tRNA with its minor bases. *Nucl. Acids Res.* **20**, 5159–5166.
53. Puglisi, J. D. & Tinoco, I., Jr (1989). Absorbance melting curves of RNA. *Methods Enzymol.* **180**, 304–325.
54. Rotondo, G., Gillespie, M. & Frendewey, D. (1995). Rescue of the fission yeast snRNA synthesis mutant snm1 by overexpression of the double-strand-specific Pac1 ribonuclease. *Mol. Gen. Genet.* **247**, 698–708.
55. Amarasinghe, A. K., Calin-Jageman, I., Harmouch, A., Sun, W. & Nicholson, A. W. (2001). *Escherichia coli* ribonuclease III: affinity purification of hexa-histidine-tagged enzyme and assays for substrate binding and cleavage. *Methods Enzymol.* **342**, 143–158.
56. Umen, J. G. & Guthrie, C. (1995). The second catalytic step of pre-mRNA splicing. *RNA*, **1**, 869–885.

Edited by D. E. Draper

(Received 12 December 2003; received in revised form 10 February 2004; accepted 14 February 2004)

Supplementary Material comprising three Figures is available on Science Direct